ICES Journal of Marine Science, 2024, Vol. 0, Issue 0, 1–15
https://doi.org/10.1093/icesjms/fsae071
Received: 8 February 2024; **revised:** 12 May 2024; **accepted:** 13 May 2024
Original Article

Acoustic observations of walleye pollock (*Gadus chalcogrammus*) migration across the US-Russia boundary in the northwest Bering Sea

Robert M. Levine [1,*], Alex De Robertis [1], Christopher Bassett [2], Mike Levine [1], James N. Ianelli [3]

[1]Resource Assessment and Conservation Engineering Division, Alaska Fisheries Science Center, National Marine Fisheries Service, National Oceanic and Atmospheric Administration, Seattle, WA 98115, USA
[2]Applied Physics Laboratory, University of Washington, Seattle, WA 98105, USA
[3]Resource Ecology and Fisheries Management Division, Alaska Fisheries Science Center, National Marine Fisheries Service, National Oceanic and Atmospheric Administration, Seattle, Washington 98115, USA

*Corresponding author. Resource Assessment and Conservation Engineering Division, Alaska Fisheries Science Center, National Marine Fisheries Service, National Oceanic and Atmospheric Administration, 7600 Sand Point Way NE, Seattle, WA 98115, USA. E-mail: Robert.Levine@noaa.gov

Abstract

The degree to which walleye pollock (*Gadus chalcogrammus*, hereafter pollock) move between the US and Russian zones of the Bering Sea is a key source of uncertainty for fisheries management. To study transboundary migrations across the US–Russia maritime boundary and explore how climate variability might influence these migrations, four seafloor-mounted echosounder moorings were deployed from July 2019 to August 2020 in the northwestern Bering Sea. The observations indicated that a substantial amount of pollock moves between the US and Russia seasonally, with a period of southeast movement into the US as winter as sea ice forms and northwest movement into Russia in early summer as waters warm. Over the deployment period, 2.3-times more pollock backscatter moved into the US zone in fall and winter than exited the subsequent spring and summer. We hypothesize that the difference in the net movement between regions was driven by pollock moving farther into Russia during the historically warm conditions at the start of deployment period and reduced northwest return migration the following summer when temperatures were relatively cooler. This supports the hypothesis that temperature affects pollock distribution, and that continued warming will lead to a larger proportion of the stock in Russian waters.

Keywords: Bering Sea; *Gadus chalcogrammus*; migration; echosounder; mooring; wideband autonomous transceiver

Introduction

Many commercially important marine species span multiple management zones and undergo transboundary movements (Meltzer 1994, Palacios-Abrantes et al. 2022). Management of such transboundary stocks can be difficult due to changes in the availability of a species because of seasonal or annual movements, resulting in competition or overexploitation (Liu and Molina 2021) and adding uncertainty to stock assessments (Currie et al. 2019, O'Leary et al. 2020). Climate change is leading to the further redistribution of species globally, resulting in new or shifting transboundary stocks (Pinsky et al. 2013, Melbourne-Thomas et al. 2022, Palacios-Abrantes et al. 2022). Changes in transboundary stocks can disrupt cooperative fishery management based on historic distributions (Miller and Munro 2004).

Walleye pollock (*Gadus chalcogrammus*, hereafter referred to as pollock) is a semi-pelagic fish widely distributed throughout the North Pacific (Bailey et al. 1999), and the second largest single-species fishery in the world by biomass (FAO 2021). The commercial harvest of pollock harvest exceeds 1 million metric tons annually in the US zone of the eastern Bering Sea (Ianelli et al. 2022), while annual harvest in the Russian zone (northwestern Bering Sea) has been approximately 0.4 million metric tons over the past two decades (Gritsay and Stepanenko 2022). The fishery is active from January to October, with peak fishing near the maritime boundary occurring from June to October. Pollock are managed separately within the US and Russian zones, and each area depends to varying degrees on fishery-independent surveys (Gritsay and Stepanenko 2022, Ianelli et al. 2022).

While the respective US and Russian management processes in the Bering Sea region have been successful, warming of the Bering Sea shelf may alter pollock distribution more than has been apparent in the past relative to historical distributions. Bottom temperatures over the entire Bering Sea exhibit seasonal patterns driven by winter cooling and ice formation. Typically, water from melted sea ice sinks to form a region of cold (<2°C) bottom water (the "cold pool") that persists through summer and fall. This cold pool is thought to serve as a thermal barrier that may limit the northward movement of subarctic species (Kotwicki et al. 2005). The cold pool extent has been identified as a key mechanism affecting the spatial distribution of pollock in the eastern Bering Sea (Kotwicki and Lauth 2013) and is used in the spatio-temporal modeling of pollock distributions (Ianelli et al. 2022). For example, warm conditions in 2017–2019 led to very small cold pool extents with warmer water in the southern portion of the shelf relative to historical temperatures (Clement Kinney et al. 2022).

During this time, the US Bering Sea summer bottom-trawl surveys found higher than normal abundances of pollock in northern areas (Stevenson and Lauth 2019, Eisner et al. 2020, O'Leary et al. 2022). Long-term observations indicate that the proportion of pollock biomass in Russia increases when the cold pool is small and conditions are warm across the shelf (O'Leary et al. 2022, Stevenson et al. 2022). Further, acoustic-trawl surveys in the Russian zone of the Bering Sea shelf have identified a correlation between bottom temperatures and pollock abundance in the Navarin and Gulf of Anadyr regions (Polyanichko and Kuznetsov 2022).

The seasonal movements of pollock remain poorly understood. Pollock appear to perform seasonal migrations between spawning grounds and feeding areas in the Sea of Japan (Maeda 1986). Similar movement patterns have been inferred for the western Bering Sea (Radchenko and Sobolevskiy 1993) and the eastern Bering Sea based on large-scale synoptic summer surveys (Wyllie-Echeverria and Wooster 1998, Kotwicki et al. 2005). Comparison of distributions during surveys in early spring and summer indicate that pollock likely retreat southeast toward the shelf slope and deeper water in the winter and spring to avoid cold temperatures (De Robertis and Cokelet 2012). While there are no direct observations of year-round seasonal movements, survey data indicate that pollock seasonal migrations likely extend across national jurisdictions within the Bering Sea (Kotwicki et al. 2005). Furthermore, the direction, timing, and magnitude of this seasonal pollock movement into the northwestern portion of the shelf is believed to be driven by temperature and sea ice (Stepanenko 2001, Kotwicki et al. 2005, De Robertis and Cokelet 2012, Gritsay and Stepanenko 2022, Polyanichko and Kuznetsov 2022).

Moored instrumentation can be deployed during the ice-free period and used to collect data year-round in remote and seasonally ice-covered regions such as the northwestern Bering Sea shelf (Kitamura et al. 2017, Levine et al. 2023) to monitor abundance near the maritime boundary. Moored echosounders have been used to collect long-term observations of fish abundance (Trevorrow 2005, Urmy et al. 2012, De Robertis et al. 2018). The use of split-beam echosounders on moored platforms facilitates the detection and tracking of individual scatterers (Kaartvedt et al. 2009, Christiansen et al. 2022), which make it possible to monitor the movement of fish populations over extended periods (Levine et al. 2023, Maathuis et al. 2023). A key limitation of such acoustic mooring observations is the lack of direct biological sampling to identify acoustic scatterers, apart from the potential opportunity to sample during the deployment and recovery events. However, in regions such as the eastern Bering Sea, where the pelagic acoustic backscatter is dominated by a single species, interpretation of the acoustic data is less dependent on biological sampling (De Robertis et al. 2018, 2021) and acoustic measurements can be used to infer the size of scatterers (Levine et al. 2021, 2023).

Here, we report on the use of seafloor-mounted echosounder moorings to collect near-continuous acoustic observations of pollock abundance and movement over the course of a year near the US–Russia maritime boundary in the Bering Sea. The primary objectives were to characterize the seasonal abundance patterns in the northwestern portion of the Bering Sea shelf and quantify movements of pollock across the maritime boundary. Population flux is estimated by combining tracking of individual fish and acoustic backscatter measurements. Additionally, acoustic target strength (TS) measurements allow estimates of how fish size distribution changed over time. We explore the potential environmental drivers of seasonal pollock distribution and hypothesize how climate variability will impact future distribution patterns.

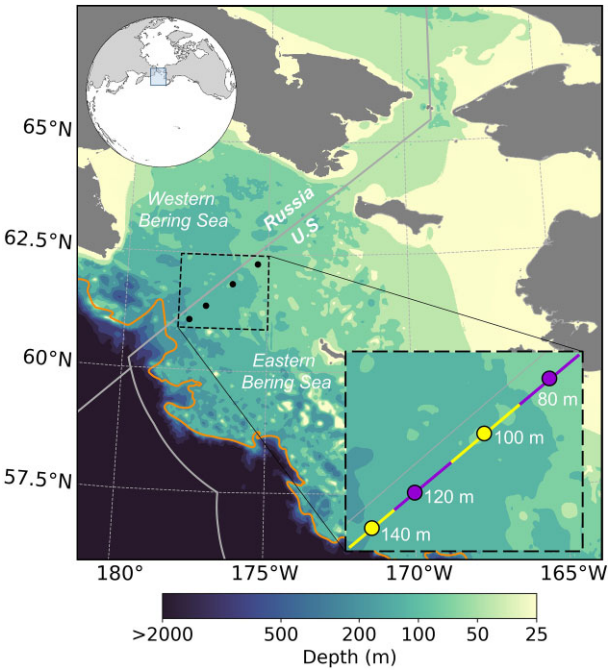

Figure 1. Map of study region. The mooring locations are indicated by the black dots. Inset map (lower right) shows the position of each mooring (purple and yellow circles) and transect segment (purple and yellow segments) along which the observations from each site were extrapolated when estimating movement. The boundaries of the US and Russian exclusive economic zones are indicated by the solid grey lines. The 200 m contour is indicated by the orange line.

Methods

Mooring deployments

Four moorings equipped with upward-looking echosounders were deployed 10 nautical miles (nmi) into the US zone in the northwestern Bering Sea parallel to the US–Russia maritime boundary at bottom depths of approximately 80, 100, 120, and 140 m (Fig. 1, Table 1). The moorings were deployed on 24–25 July 2019 and recovered on 06 September 2020. The moorings were positioned along a line such that the combined extrapolated observations from the four moorings would be used to compute the movement across a larger transect representing bottom depths from 70 to 150 m (see inset, Fig. 1). The mooring locations were selected based on an analysis of 11 years of summer acoustic-trawl survey observations conducted by the NOAA Alaska Fisheries Science Center in the northwestern Bering Sea between 2004 and 2018, which indicate that on average, 63.4% (41.2%–85.6%) of backscatter attributed to pollock on the surveys is typically found in the midwater between the 70 and 150 m isobaths (Fig. S1; McCarthy et al. 2020).

The moorings (described in De Robertis et al. 2018) were instrumented with battery-powered echosounders (Wideband Autonomous Transceiver, Simrad AS) and 70 kHz, 18°

Table 1. Mooring site bottom depth, location, mean compass heading and magnetic declination used when correcting track direction, and transect segment length (d_i, see Methods).

Site	Bottom depth (m)	Latitude	Longitude	Compass heading	Magnetic declination	Segment length (km)
80 m	77.3	62.2903	−175.3713	54.8°	4.3°	66.6
100 m	95.6	61.85022	−176.25066	77.0°	3.8°	69.4
120 m	116.3	61.36881	−177.17	71.7°	3.4°	58.8
140 m	136.7	61.06918	−177.73993	152.5°	3.1°	45.3

depth-rated split-beam transducers (ES70-18CD). The echosounders transmitted a 0.512 ms, 70 kHz narrowband pulse with a power of 300 W. The transducers were mounted in a two-axis gimbal equipped with a 0.7 kg counterweight such that the face of the transducer was 0.6 m above the seafloor and remained oriented toward the sea surface.

The echosounders were programmed to record data from 26 July 2019 to 31 August 2020. An ensemble of 320 pings at 2 pings s^{-1} was transmitted every 2 hours (2% duty cycle). Data were recorded to 155 m range to ensure data collection past the range of the sea surface. The echosounders were calibrated prior to deployment at the surface using a 38.1 mm tungsten-carbide standard sphere (Demer et al. 2015). The gains among all echosounders were similar, with an average gain of 19.76 (± 0.19 SD) dB. Post-deployment testing indicated that the average target strength (TS, dB re 1 m^2) of a calibration sphere varied by <15% at deployments depths of 100–140 m relative to the surface, consistent with previously reported investigations of depth-dependence in ES70-18CD transducers (Levine et al. 2023). To determine the transducer heading once the moorings settled on the seafloor, each mooring was equipped with a compass (OpenTag, Loggerhead Instruments) calibrated on the fully assembled moorings to account for the impact of any ferrous material. The mode of all heading observations from the time the mooring settled on the seafloor until the compass batteries were exhausted (~8 d), corrected for local magnetic declination, was used to represent the mooring orientation on the seafloor (Table 1) when computing the direction of fish tracks (described below) relative to the maritime boundary.

Interpreting acoustic backscatter

The eastern Bering Sea is a region of low pelagic diversity which makes interpretation of acoustic backscatter without simultaneous direct biological sampling less uncertain (De Robertis et al. 2021, Levine et al. 2023). Walleye pollock dominate the backscatter in the eastern Bering Sea in the summer (McCarthy et al. 2020). Large-scale acoustic indices in the eastern Bering Sea are highly correlated with acoustic-trawl survey biomass estimates for walleye pollock (De Robertis et al. 2021) and are used in the stock assessment for the fishery (Honkalehto et al. 2011, Ianelli et al. 2020). Research and commercial trawls targeted on pollock aggregations in the eastern Bering Sea exhibit little bycatch (>98% pollock by weight, De Robertis et al. 2021). Backscatter in the immediate vicinity of the moorings is also dominated by pollock in summer; in the 11 summer acoustic-trawl surveys of the eastern Bering Sea conducted since 2005, the proportion of all backscatter observed within 60 nmi of the maritime boundary that was attributed to pollock was >80% in seven surveys and >95% in four of those years (Fig. S2, data from De Robertis et al. 2021). The backscatter not attributed to pollock is generally found in the upper 40 m of the water column and tends to form identifiable diffuse layers, allowing for high confidence in identifying pollock backscatter during visual inspection (De Robertis et al. 2021). During periods of low backscatter on the shelf (e.g. early spring, De Robertis and Cokelet 2012), uncertainty increases in the composition of sound-scattering organisms. However, these latter periods likely contribute only a small portion of the overall backscatter. Therefore, when backscatter is high, we assume that pollock are the primary contributors to backscatter and that acoustic-based measures of fish density reflect their abundance and distribution.

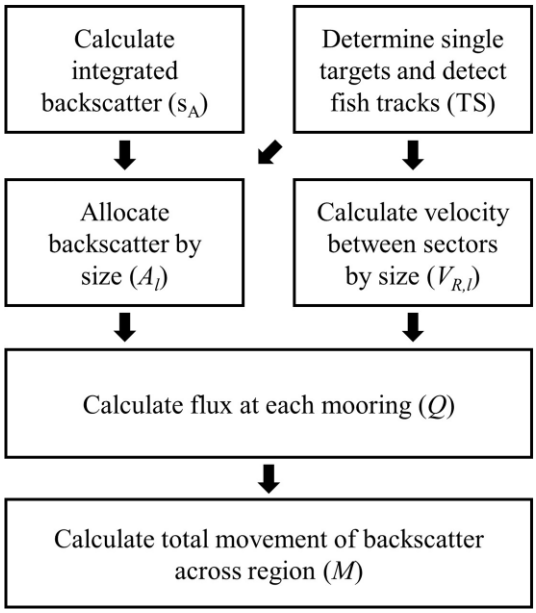

Figure 2. Analysis workflow with the key output at each step indicated in parentheses.

Processing of acoustic data

Integrated water column backscatter was combined with target tracking of individual fish to estimate the movement of pollock backscatter across the mooring transect (Fig. 2). After calculating total backscatter attributed to pollock, single-target detections were assembled into tracks from which we estimated the size distribution and horizontal displacement of scatterers. From the track speeds and direction, we calculated the velocity component of the tracks perpendicular to the mooring transect. This velocity was combined with backscatter to calculate the movement of backscatter across the mooring transect, representing movement across the US–Russia maritime boundary.

Acoustic data were processed using Echoview 13 (Echoview Software Pty Ltd) following the methods described in Levine et al. (2023) and summarized below. The echo from the sea surface/ice was determined using Echoview's threshold offset operator with a minimum detection threshold of −50 S_v (dB re 1 m^{-1}) below the surface/ice and manually corrected after visual inspection. As part of the visual inspection, water column backscatter was vertically partitioned into pollock backscatter or as an unclassified category. This unclassified category was used to indicate near-surface low confidence regions of unknown scatterers. At all sites, the unclassified scattering composed 3%–6% of the total backscatter observed over the course of the deployment, with 92%–98% of the unclassified scattering in the upper 30 m (Fig. S3). During the months of the summer acoustic-trawl surveys (July and August), unclassified scattering composed 12%–20% of the total backscatter. These summer observations are consistent with survey data within 60 nmi of the maritime boundary, where >80% of the backscatter has been attributed to pollock in seven of the past 11 surveys (Fig. S2). The nautical area scattering coefficient (s_A, m^2 nmi^{-2}) was computed from 2 m above the transducer to 2 m below the surface in 1 m bins for every ensemble. Although the quantities were almost interchangeable, we, hereafter, refer to data from the backscatter attributed to pollock as pollock backscatter and the sum of both pollock and unclassified categories as backscatter.

To identify day–night differences in pollock backscatter due to diel vertical migration, solar altitude was calculated for every ensemble based on the date/time and location of each mooring using the Pysolar library for Python (http://pysolar.org). Day–night differences in vertical distribution of pollock backscatter were quantified by calculating the weighted mean depth of the backscatter for the entire water column in each ensemble (Eq. 2 in Woillez et al. 2007). Paired *t*-tests were used to identify differences in weighted mean depth and pollock backscatter between daily daytime and nighttime ensembles at each site.

Fish track detection

Echoes from individual scatterers in backscatter classified as pollock were identified with Echoview's split-beam single target detection (method 2), using a detection threshold of −70 dB re 1 m^2 (see Table S1 for detection parameters). Individual fish trajectories were assembled from single targets using Echoview's 4D alpha-beta tracker (Table S2; Blackman 1986). A minimum of five detections from an individual was required to classify a track, with a maximum gap of five pings (2.5 s). The mean TS of each track was calculated as $10\log_{10}(\bar{\sigma}_{bs})$ where $\bar{\sigma}_{bs}$ (m^2) is the mean backscattering cross-section. To further restrict the inclusion of non-pollock scatterers in velocity and flux estimates, only tracks where mean TS ≥ −55 dB re 1 m^2 (corresponding to a 3.5 cm pollock, Traynor 1996) were included in further analyses.

Estimating size-dependent contribution to backscatter

A Gaussian mixture model (GMM) was applied to target-strength frequency data to estimate the size distribution of the acoustically observed pollock during each semi-monthly period (beginning on the 1st and 16th of every month). GMMs are probabilistic models for representing individual components of a population where each component is approximated by a normal distribution (McLachlan and Peel 2000). GMMs can be used to estimate the contribution of n component classes to the overall distribution, such as the contribution of different size-/age-classes to the structure of a population (Shaw et al. 2021). We used an expectation–maximization algorithm to predict the optimal mixture weights for pollock size classes using TSs corresponding to 1-cm length bins ranging from 2 to 60 cm by maximizing log-likelihood.

The probability of the TS distribution for each period can be represented as

$$f(x) = \sum_l w_l \times g(x|\mu_l, \sigma), \tag{1}$$

where $f(x)$ is the overall TS distribution, w_l is the mixture weight at length l, and $g(x|\mu_L, \sigma)$ is the normally distributed probability density function for the distribution of length bin l given the expected mean TS μ_l and variance σ. Analysis of 16 periods with a unimodal TS distribution suggestive of a narrow size range was used to empirically estimate a value of $\sigma = 3.6$ dB re 1 m^2 which was used to calculate the mixture weight at length during each period at each mooring site. To account for difference in both aspect (ventral vs. dorsal view) and frequency (70 kHz rather than 38 kHz), a modified TS-length relationship for pollock (Traynor 1996) was used, such that

$$TS_l = 20\log_{10}(l) - (66 + 10\log_{10}(1.32)) \tag{2}$$

using the $10\log_{10}(1.32)$ ship-to-mooring ratio reported in De Robertis et al. (2018) to account for the frequency and orientation differences between the mooring observations and those assumed in the TS relationship. The proportion of the pollock backscatter (PB) attributed to pollock of length l during each period t at each mooring site i was calculated as

$$PB_{l,t,i} = \frac{\sigma_{bs,l} w_{l,t,i}}{\sum_l \sigma_{bs,l} w_{l,t,i}}, \tag{3}$$

where the expected backscattering cross-section for each length class $\sigma_{bs,l}$ is

$$\sigma_{bs,l} = 10^{\frac{TS_l}{10}}. \tag{4}$$

Thus, the total pollock backscatter A (m^2 m^{-2}) attributed to each length class is

$$A_{l,t,i} = PB_{l,t,i} \times s_{A,t,i} \times \frac{1}{4\pi \times 1852^2}, \tag{5}$$

where the $4\pi \times 1852^2$ term accounts for the conversion between nautical area backscattering (s_A, m^2 nmi^{-2}) to the area backscattering coefficient (s_a, m^2 m^{-2}).

Calculating track velocity

The velocity of individual scatterers was calculated following Levine et al. (2023) as summarized below. Since the objective was to calculate horizontal displacement, track headings and speeds were calculated in two dimensions by fitting two-dimensional linear models with respect to time for the x, y positions of the single-target detections in each fish track. Headings were converted from a coordinate system relative to the transducer into a geographic reference frame based on the compass orientation.

For each track j, we computed the velocity component of each track along the axis perpendicular to the maritime

boundary ($V_{R,j}$) using the speed (S_j) and heading (H_j) calculated from the linear model projection of the track as

$$V_{R,j} = S_j \times \cos\left((H_j - \theta)\frac{\pi}{180}\right), \quad (6)$$

where $\theta = 312^\circ$, the heading perpendicular to the mooring transect toward Russia. Velocity for each semi-monthly period of observations was calculated for each 1-cm length bin l from 2 to 60 cm. The speed of fish tracks was TS-dependent, with higher TS values (i.e. larger fish; 2) corresponding to higher track speeds (Fig. S4). To account for this size-dependence, the mean velocity toward Russia at each length $\overline{V_{R,l,t,i}}$ was calculated by fitting a linear regression of $V_{R,j,t,i}$ to $l_{j,t,i}$ (Fig. S5). To reduce the influence of a limited number of small or large scatterers on the slope of individual bi-monthly regressions, regressions were fit after removing the lower and upper 2.5% of tracks based on mean track TS. Tracks with a TS outside this interval were assigned the same speed as the track with the closest mean TS used to fit the regression (Fig. S5).

Estimating flux and total movement

Flux was estimated in units of backscatter crossing the US–Russia maritime boundary. While the GMM was used to identify temporal changes in pollock size, the uncertainty in these estimates remains to be characterized. It is unclear how this uncertainty in the resulting length distributions would influence a backscatter-to-biomass conversion. Pollock weight scales as the cube of pollock length, therefore small errors in estimates of size distribution have the potential to have a large impact on any subsequent calculation of biomass. Thus, we chose to compute flux in units of backscatter rather than biomass.

Using the length-dependent velocities and backscatter, the length-dependent flux of pollock backscatter across the US–Russia maritime boundary (Q_R, $m^2\ m^{-1}\ s^{-1}$) was calculated as

$$Q_{R,l,t,i} = A_{l,t,i} \times \overline{V_{R,l,t,i}}, \quad (7)$$

where $Q_{R,l,t,i}$ represents the mean backscatter from scatterers of size l crossing a 1-m line parallel to the border in 1 s during period t at mooring site i. To estimate the total movement across the transect line represented by the mooring locations, the observations at each mooring site were applied over a distance d (m) equal to the inter-mooring distance on each side (Fig. 1, Table 1). At the 80 and 140 m sites, the distance extrapolated for each mooring was equal to twice the inter-mooring distance to the nearest mooring. This assumes that the measurements at each location are representative of the conditions across the distance over which the value is applied, roughly corresponding to each mooring representing data within ±10 m of its deployment depth. The total movement of pollock backscatter (M, m^2) during each period across the transect (Fig. 1) was calculated as

$$M_{l,t} = \sum_i Q_{R,l,t,i} \times T_t \times d_i, \quad (8)$$

where T_t is the duration of period t in seconds. The total movement during each period (M_t) was then calculated by summing backscatter over all length classes.

Uncertainty in total movement attributable to temporal variability in the observations was estimated via a two-step bootstrap process. First, 300 sets of total movement calculations were drawn for each mooring site. In each iteration, n ping ensembles from each semi-monthly period were selected at random with replacement, where n was the total number of ping ensembles collected within that period. Flux at each site was calculated from the backscatter and tracks within the selected ensembles, including recalculation of the contribution of backscatter by size (3, 5) and length-dependent velocities (6–7). Next, 10 000 bootstrap estimates of total movement for each semi-monthly period were calculated by randomly drawing one of the 300 bootstrapped flux estimates from each mooring and then estimating total transport across the mooring transect (8). Approximate 95% confidence intervals were estimated by finding the 2.5 and 97.5 percentiles of total movement M from the 10 000 iterations.

Environmental correlations with pollock movement

We used observations and model estimates of temperature, salinity, and sea ice cover to investigate the potential influence of the environment on pollock movement across the maritime boundary. Bottom temperatures were available from a sensor deployed on each mooring (Sea-Bird Scientific SBE-37 or SBE-56). Mean water column temperatures were obtained from the output of a 10 km horizontal resolution implementation of the Regional Ocean Modeling System (Shchepetkin and McWilliams 2005) for the Bering Sea (Bering 10K, Hermann et al. 2019). To represent the temperatures in the mooring region, we spatially averaged all observations within a rectangular portion of the Bering Sea shelf encompassing the moorings where the lower left and upper right corners are the locations of the southwest and northeast ends of the mooring transect, respectively (dashed box in Fig. 1). To identify patterns in relation to seasonal sea ice, we obtained ice concentrations from the MASIE-AMSR2 (MASAM2) Daily 4 km Arctic Sea Ice Concentration, Version 2 (Fetterer et al. 2023). The daily measurement from the nearest 16 km^2 grid cell was used to represent conditions at each mooring site.

Results

Seasonality of backscatter

Seasonal changes in acoustic backscatter were consistent at all four sites, with variability in the seasonal timing of departure/arrival of backscatter as a function of depth. The colder shallower sites (80 and 100 m) exhibited earlier departure and later arrival of scatterers than the deeper sites (120 and 140 m) (Fig. 3). Backscatter was high at all mooring sites in early winter when bottom temperatures were still warm (December–January, Fig. 3). During this period, pollock backscatter was greatest at the deeper (120 and 140 m) sites (largest 7-day moving average nautical area backscattering [s_A, $m^2\ nmi^{-2}$]: 2297 at 80 m, 2654 at 100 m, 3039 at 120 m, and 5106 at 140 m; Fig. S6). Backscatter began to decrease shortly afterward, with little backscatter remaining at the shallow (80 and 100 m) sites by mid-February and deeper (120 and 140 m) sites by mid-March. Backscatter began to increase in late spring. Midwater and shallow scattering layers developed at the deeper sites in early May, reaching the same level of backscatter in June as was observed the previous summer. The reappearance of high backscatter occurred later, in late May and mid-June, at the 100 m and 80 m sites.

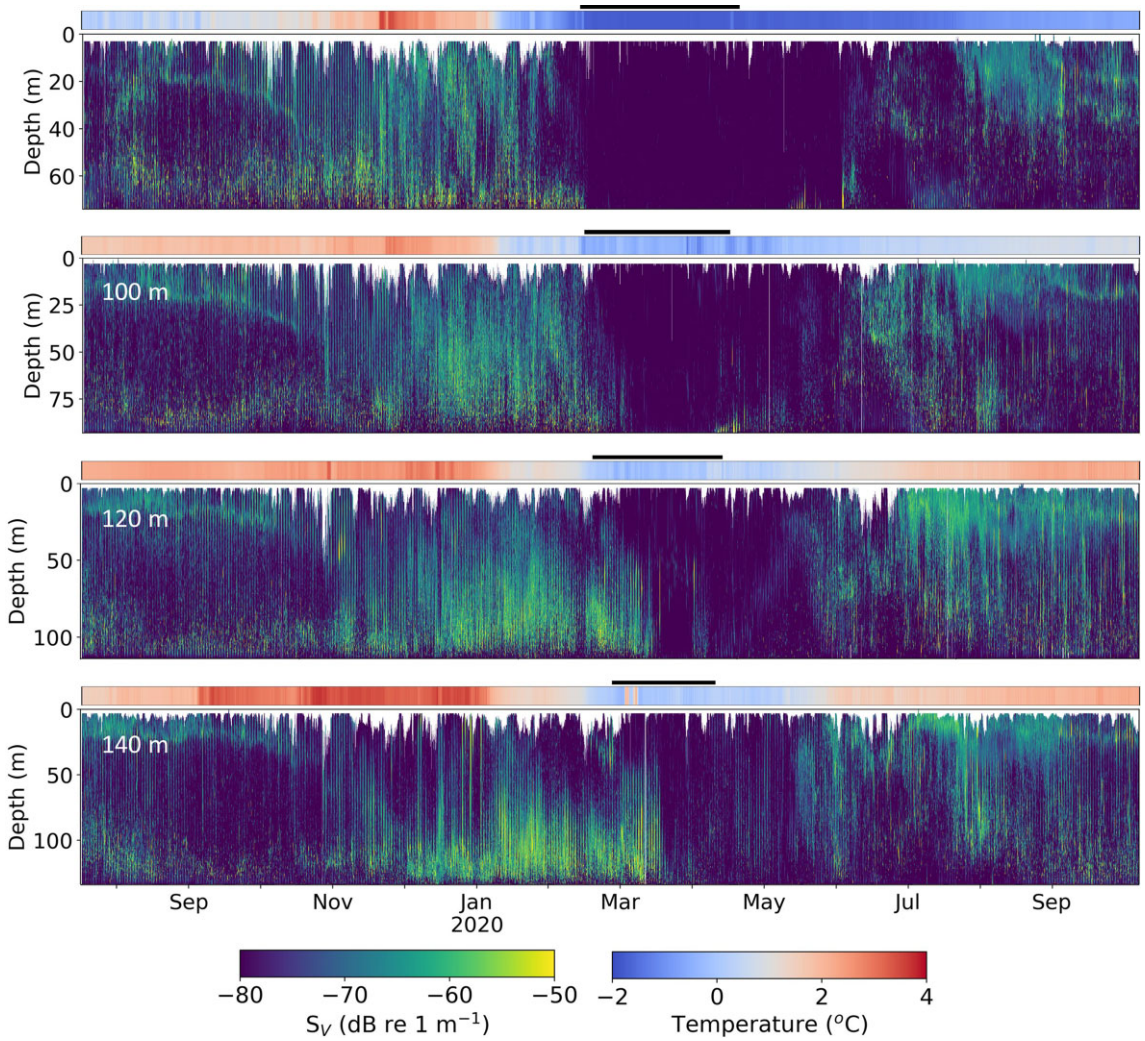

Figure 3. Echograms of 70 kHz backscatter at the 80 m, 100 m, 120 m, and 140 m mooring locations. Each data point represents the mean volume backscattering coefficient (S_V) for each 2-h ensemble in a 1-m bin of the water column. White portions indicate where backscatter from the sea surface/ice and noise have been removed. The heat map above each echogram show the bottom temperature recorded by the CTD on each mooring, and the black line indicates the period between the first and last day when ice coverage exceeded 20%.

Overall, pollock backscatter tended to be greater at night than during the day, although this difference was only significant (paired *t*-test, $P < 0.01$) at the 100 m [21 ± 8% (mean ± 95% CI)] and 120 m (15 ± 6%) sites. This increase in nighttime pollock backscatter is likely associated with nighttime upward movement of scatterers into the observed area from the unobserved near-bottom zone, which is consistent with the diel vertical migration of fish. Pollock backscatter was significantly deeper during daytime at all sites (weighted mean depth values across sites were 7.8–16.8 m deeper during the day; paired *t*-test, $P << 0.001$). Median depth of pollock backscatter was 25–28 m off-bottom during the day at all sites and up to 50 m off-bottom at night (Fig. S7).

Patterns in size distribution

There was a strong seasonality in the distribution of the mean track TSs (Fig. 4). The size of pollock that dominated the backscatter also varied consistently over each of the sites. A total of 551 285 tracks were reconstructed from single target measurements over the course of the deployment at all four sites (77 363 at 80 m, 120 666 at 100 m, 160 376 at 120 m, and 192 880 at 140 m). Tracks were detected throughout the water column at each site (Fig. S8). Track depths were consistent with the vertical distributions of backscatter (Figs S3). On average, more tracks were detected at night (17%–40% more per unit time depending on site), likely because the fish were more dispersed. The observed TSs were consistent with those expected from pollock; the median TSs across all sites during each semi-monthly period varied between −54 and −30 dB re 1 m^2, corresponding with pollock lengths from 4 to 61 cm (Fig. 4).

Patterns in inferred size distribution were consistent among sites and align with the seasonal transitions in backscatter. Beginning in July 2019, relatively high TSs, consistent with those of age 2+ pollock, were observed at all sites, with median values between −40 and −33 dB re 1 m^2 in August (Fig. 4). From August to November, these high TS tracks became less prevalent, and the median TS during this period decreased as a second mode of weaker TSs, consistent with

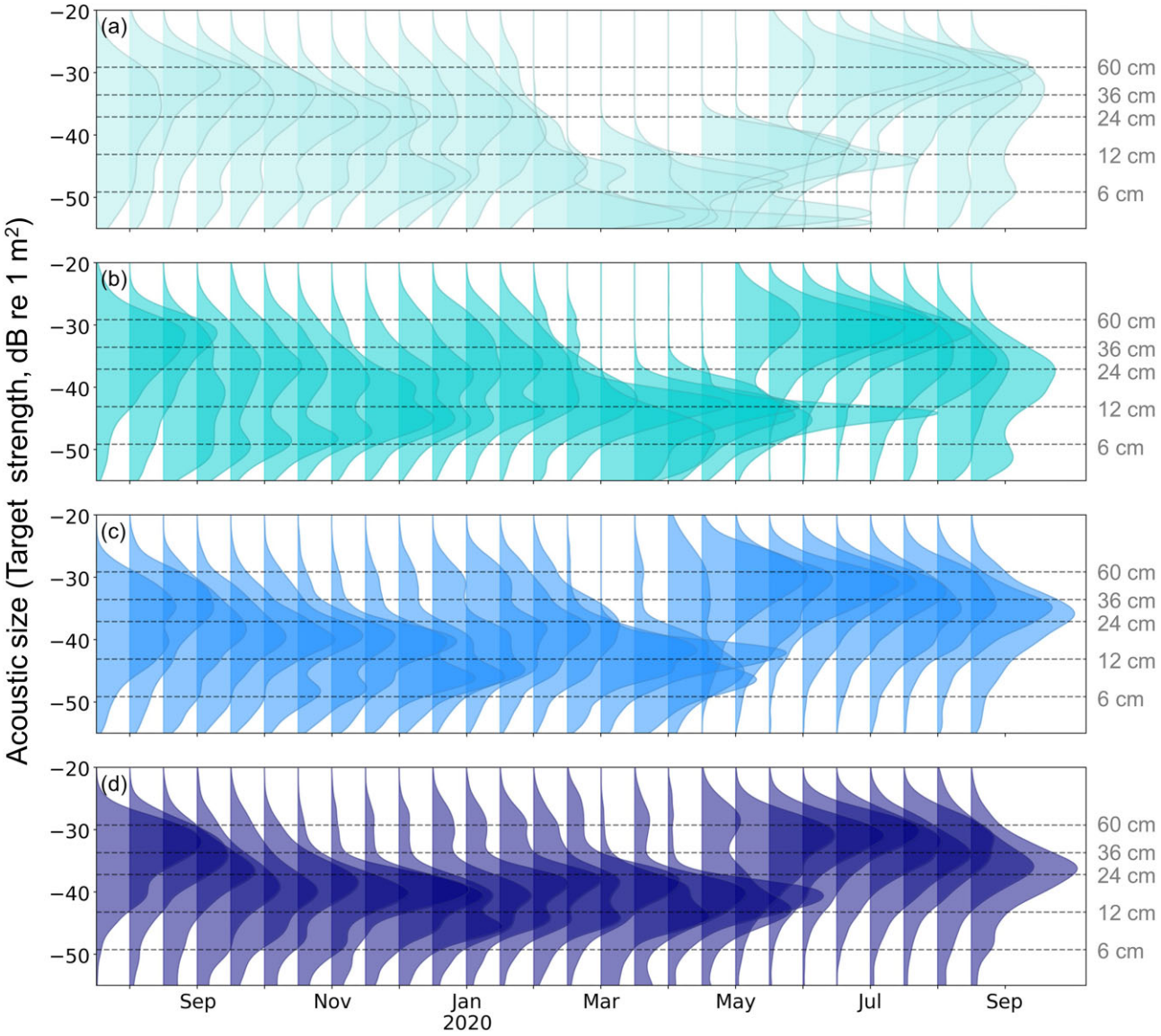

Figure 4. Time series of changes in distribution of target strength (TS) over the course of each deployment at the (a) 80, (b) 100, (c) 120, and (d) 140 m mooring locations. Each distribution is the kernel density estimate of all track mean TSs within each semi-monthly period and is represented as a probability density (i.e. normalized such that it sums to one). Dashed horizontal lines indicate reference lengths for pollock based on TS-length relationship (see Methods, Equation 2).

young-of-the-year pollock (∼−50 dB re 1 m^2), appeared at all sites (Fig. 4). Beginning in December, higher TS (∼−30 dB re 1 m^2) tracks, consistent with larger adult pollock, became more prevalent at all sites, corresponding with the period of high backscatter which occurred in early winter and persisted until late February, especially at the deeper sites (Fig. 3).

In March and April, when backscatter was low, few tracks were present, especially at the shallower sites; this period only accounted for 0.5% of tracks at the 80 m site and 4.5% of tracks at the 100 m site. Target strengths at those moorings were low and highly variable, primarily within the range of TSs expected for small fish such as age-0 gadids (Levine et al. 2023). At the 120 and 140 m sites, the number of tracks during this period was also low (2.2% and 11.2% of all tracks), but TSs remained consistent with the weaker (−45 dB re 1 m^2) mode that had appeared earlier in the fall.

As backscatter increased in May and June (Fig. 3), the distribution of TSs shifted to a single higher value mode at all sites (Fig. 4), with median values consistent with those expected for 40–50 cm adult pollock. These estimated sizes are consistent with catches in the Russian pollock fishery (mean of 44.8 cm with peak fishing in June and July 2020; Gritsay and Stapenanko 2022). In July and August, there was an increase in the scatterers corresponding to ∼30 cm pollock (Fig. 4). These TS distributions were similar to those observed on the same dates in the previous year.

Movement of pollock

Daily mean horizontal track speeds were consistent among all four moorings (24.5–26.4 cm s^{-1}, Fig. S9a). When calculated relative to the maritime boundary, the absolute daily mean velocity component perpendicular to the mooring transect was

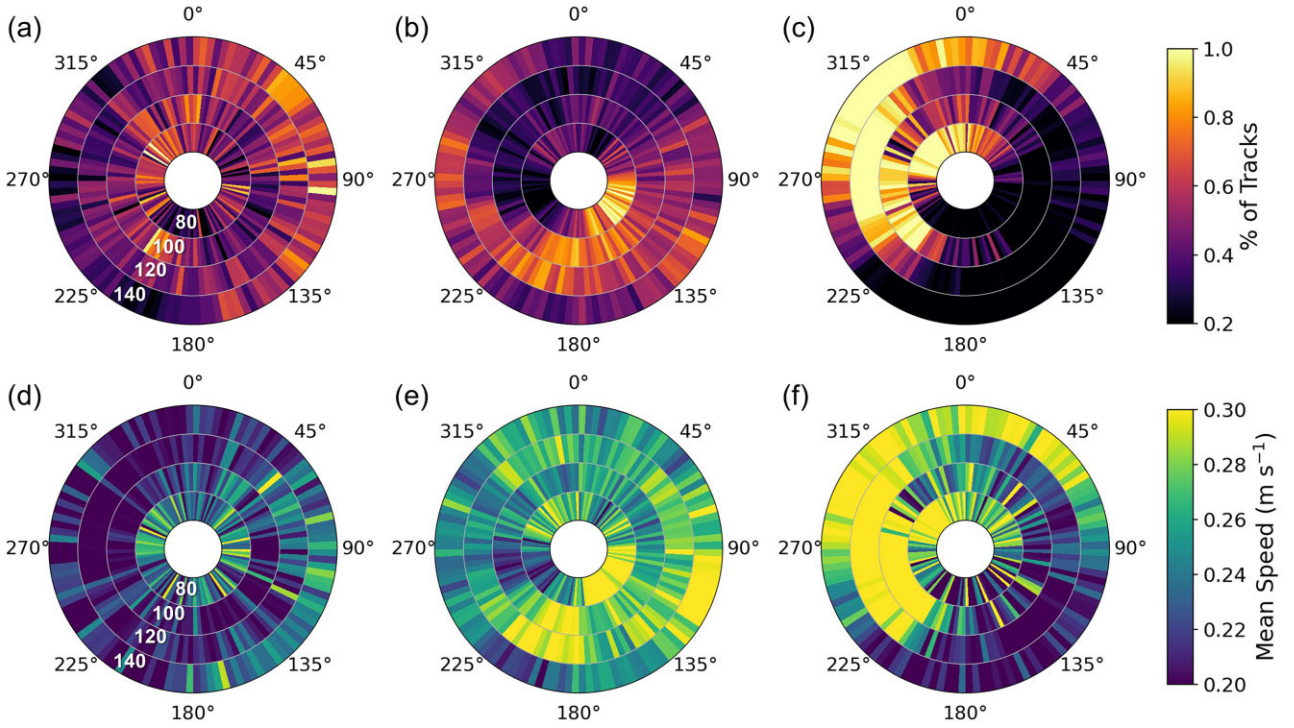

Figure 5. Polar representations of (a–c) the distribution of track headings and (d–f) mean speeds (m s^{-1}) at all four mooring sites during select semi-monthly periods representing (a, d) late summer, (b, e) winter, and (c, f) spring movement patterns. The innermost band shows the tracks observed at the 80 m site and subsequent bands representing the next deepest location with the outermost band showing the tracks at the 140 m site. (a, d) 1–15 September 2019, (b, e) 1–15 January 2020, and (c, f) 1–15 May 2020. The color indicates the (a–c) percentage of tracks with horizontal headings and (d–f) mean speed of tracks within the 15-day window within each 3° bin during that time period.

15.5–17.4 cm s^{-1} with a net mean velocity across the transect of <0.02 cm s^{-1} at all sites (Fig. S9b).

The flux of pollock backscatter across the maritime boundary varied seasonally. From July to November of 2019, pollock backscatter was moderately high at all four moorings (Fig. 3), but the speed of tracks was relatively low with minimal directionality (Fig. 5a, d). As a result, net movement between zones was limited during the summer and fall period (Fig. 6). Beginning in December of 2019 and continuing until early March, track headings became more directional with more tracks towards the southeast (Fig 5b). These tracks moving southeast moved faster than those moving in other directions (Fig. 5e). This increase in velocities into the US zone corresponded with an increase in backscatter at all four sites as temperatures began to decline (Fig. 3), resulting in increased movement into the US zone in winter (Fig. 6).

In March and April, transboundary movement was low (Fig. 6) and pollock backscatter was low at all sites (Fig. 3). In May, pollock backscatter began to increase (initially at the deeper sites with warmer bottom waters, see Fig. 3) and track headings were highly directed westward with relatively fast speeds (Fig. 5c, f). Movement at all sites was toward the Russian zone, with most of the northwestward movement occurring at the 100 and 120 m sites (Figs 5c, 6). While track headings and speeds indicate movement toward the Russian zone (Fig. 5c, f), this "return" of pollock backscatter was not as apparent at the 80 m site as in deeper locations due to the relatively low backscatter at 80 m in spring and summer 2020 (Fig. 3). The directed movement at the 140 m site into Russia appeared to occur primarily during a brief period in early May, while the movement into Russia at the 100 and 120 m sites continued into July (Fig. 6). Later in the summer, pollock backscatter then exhibited similar patterns to summer of 2019 where net movement, even during periods of high pollock backscatter, was low due to low directivity in the tracks.

Overall, we estimate the net movement of pollock backscatter across the 240.1 km portion of the shelf represented by the 4-mooring transect was 2.7×10^6 m^2 into the US zone of the shelf during the deployment period. Movement was highly seasonal with migration towards the US zone in winter (net movement of 4.7×10^6 m^2 into the US zone before 1st April 2020), and toward Russia in summer (net movement of 2.0×10^6 m^2 into the Russian zone after 1st April). Most of this movement was driven by the observations at the deep mooring sites; 65.3% of the net movement of pollock backscatter into the US zone occurred at the 140 m site. Using the TS of tracks as a proxy for size (Fig. 4), the majority of pollock backscatter movement at all sites was driven by larger individuals; 82.1% of the net movement into the US was estimated to be driven by tracks with TSs consistent with adult pollock >45 cm in length (Figs. 4, S10). The direction of movement across the boundary appeared to be associated with the changes in temperature over the period measured, with differences in net movement observed at each site (e.g. divergent directions between shallow and deep sites in November–December, Fig. 6) likely the result of the spatial heterogeneity of environmental conditions between sites. Movement was into the US when mean water column temperature decreased over the course of the semi-monthly period (calculated from the difference between temperature on the first and last day of each period), but movement was into Russia during periods when temperatures increased (Fig. 7).

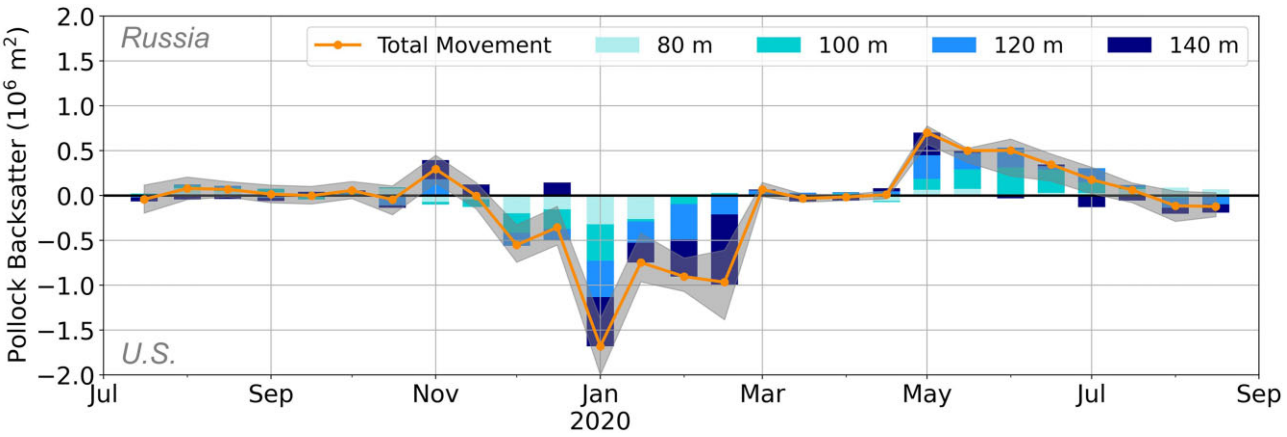

Figure 6. Net movement of pollock backscatter (m^2) across the US–Russia maritime boundary. Semi-monthly periods with positive values indicate movement into Russia and those with negative values indicate movement into the US. The stacked bars indicate the contribution to total movement of backscatter from each mooring. The orange line indicates the sum of the movement across all moorings. The gray shaded region indicates the bootstrapped 95% confidence intervals.

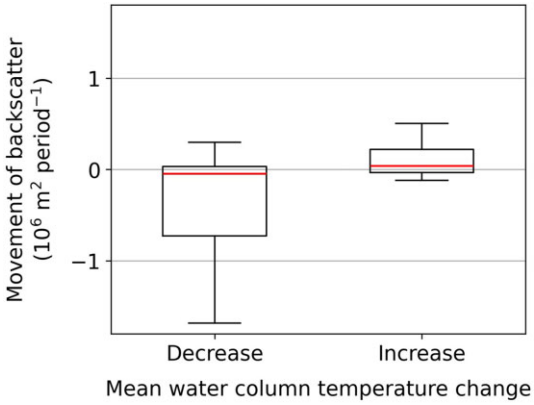

Figure 7. Distributions of movement of backscatter during semi-monthly periods when mean water column temperature over the duration of the period of observations (left) decreased and (right) increased. Water temperatures were calculated from the average conditions at the start and end of each period within a rectangular portion of the Bering Sea shelf across both zones encompassing the moorings, where the lower left and upper right corners are the locations of the southwest and northeast ends of the mooring transect, respectively (dashed box in Fig. 1). Boxes indicate the interquartile range, horizontal red lines the median, vertical lines the 5% and 95% intervals. Negative movement values imply movement into the US and positive values imply movement into Russia.

Discussion

Exchange between zones

The mooring observations suggest that a substantial proportion of the pollock stock moves across the US–Russia maritime boundary on a seasonal basis. In winter, 4.7×10^6 m^2 of pollock backscatter moved past the moorings into the US and 2.0×10^6 m^2 moved into Russia the following summer. This is comparable to the total pollock backscatter observed in summer surveys of the entire US eastern Bering Sea shelf ($1.3–4.7 \times 10^6$ m^2, De Robertis et al. 2021). During the mooring deployment period, there was thus a net movement of 2.7×10^6 m^2 into the US. The confidence intervals of the bootstrap analysis are relatively small, indicating that variability of the observations is unlikely to account for the large net movement.

Several factors may contribute to the relatively large discrepancy in the net amount of pollock backscatter that moved past the moorings toward the US compared with Russia over an annual cycle. While the mooring transect was designed to span depth ranges where the majority of the pollock backscatter has been observed on summer surveys, the moorings do not cover the entirety of the shelf, and pollock may have migrated into Russia at shallow depths to the north or within deep water along the slope.

An additional consideration is that the pollock fishery may have removed a sizeable fraction of pollock during the winter months. Using fishery catch-at length data (Ianelli et al. 2022) and pollock TS (Traynor 1996), we estimate that the 6.4×10^5 t of pollock harvested in the US zone of the Bering Sea in early 2020 equated to only 0.7×10^6 m^2 of backscatter, far less than the observed discrepancy in exchange across the maritime boundary. Thus, pollock removals in US waters during the winter 2020 fishery are insufficient to account for the large difference in backscatter between the large winter migration into the US and subsequent smaller migration into Russia.

The net movement across the boundary was high compared to previous observations of pollock backscatter from acoustic-trawl surveys that extended into Russia. In nine of the US acoustic-trawl surveys that covered a portion of the Russian zone (all prior to 2014), only 1%–30% of the total backscatter was attributed to the Russian portion of the shelf (Levine and De Robertis 2019). It is possible that pollock abundance in the Russian portion of the shelf has increased due to warming, as it has in the northern Bering and Chukchi Seas (Eisner et al. 2020, Maznikova et al. 2023). Additionally a greater proportion of pollock may be pelagic during the period of the winter migration, contributing to greater backscatter than observed in these summer surveys.

Most of the exchange of pollock across the maritime boundary occurred during winter, when the highest backscatter was observed at the mooring sites. Backscatter was much greater in winter than in summer when the acoustic-trawl surveys occur; the mean nautical area backscattering (s_A) across all four moorings was 1.7-times higher in January than August 2020. Active migration of pollock to remain within favorable environmental conditions may have led to the dense

aggregations observed in winter. When ice is present, pollock remain abundant in the marginal ice zone on the eastern Bering Sea shelf as long as bottom temperatures remain warm (De Robertis and Cokelet 2012). We observed high pollock backscatter in this portion of the shelf after sea ice concentrations had already exceeded 20%, and the period just prior to the arrival of sea ice was when some of the highest backscatter observations occurred (Fig. 3). Thus, the higher backscatter associated with the arrival of the sea ice may be the result of aggregation of the population as pollock moved toward the US zone to remain in warmer water ahead of the forming ice edge.

Changes in vertical position in winter may have led to a greater portion of the population present in the depths sampled by the echosounder. Pollock are semi-pelagic and a proportion of the biomass may be close to the seafloor where detection by acoustic surveys is more limited (Ona and Mitson 1996). Model-estimated densities of pollock biomass indicate that 12%–66% of pollock survey biomass in the eastern Bering Sea is within 0.5 m of the seafloor (Monnahan et al. 2021). We note that this is outside of the detectable range of ship-based acoustic observations and the moorings used in this study. However, changes in behavior in response to reduced light availability and other variations in the environment may lead to pollock being shallower in the water column in winter (Kotwicki et al. 2009). The moorings observed a greater amount of backscatter shallower in the water column during the winter than in summer (Fig. 3), which may indicate that pollock are coming higher off bottom and result in a larger portion of the stock in the observable range of the moorings. The change in vertical position may bias our flux estimates to indicate more movement in winter relative to spring and summer due to the availability of a larger fraction of the pollock population to the acoustic instrumentation.

Similarly, the ontogenetic transition of smaller age-0 pollock away from surface waters as they grow may also have contributed to the observation of greater pollock backscatter in winter than summer. Age-0 pollock are typically distributed near the surface in summer, moving deeper in the water column over the course of their first year of growth (Parker-Stetter et al. 2015). Of the 12%–20% of the backscatter categorized as unclassified backscatter in summer, a large portion is likely from shallow age-0 pollock as observed during summer acoustic-trawl surveys (De Robertis et al. 2021). As these individuals moved deeper later in the year, they likely transitioned to the region of the water column assigned to pollock backscatter. However, these age-0 fish have a much higher backscatter to biomass ratio than larger individuals (De Robertis et al. 2021). Thus, age-0 pollock migrating into the strata assigned to pollock may contribute to a large increase in pollock backscatter, but only a small change in biomass. Although there is substantial uncertainty in whether the availability of pollock to acoustic observations increased in winter, the large magnitude of the exchange of backscatter in both winter and summer relative to survey observations indicates that there is a sizeable exchange of pollock across the border.

Evidence of behavior-driven movement

The speed and direction of fish tracks indicate that the observations at our moorings along the US–Russia maritime boundary likely represent active migration (i.e. behavior) rather than passive transport. The moorings measured the average displacement of individuals, which includes the combined effect of directed swimming behavior and advection. If the observed migration was primarily driven by advection, one would expect tracks and currents to be consistent with each other, both in magnitude and direction, as has been observed in highly advective systems where passive transport is the principal cause of movement (Levine et al. 2023, Maathuis et al. 2023). However, the tracks observed in this study are inconsistent with the expected currents in the region. In particular, currents in this area of the shelf are typically much slower (<5 cm s^{-1}, Danielson et al. 2014, Stabeno et al. 2016) than the observed fish tracks (daily mean horizontal speeds of 24.5 to 26.4 cm s^{-1}, Fig. S9a).

The NOAA Pacific Marine Environmental Laboratory (PMEL) maintains a long-running time series of year-round acoustic Doppler current profiler (ADCP) current observations at the M8 mooring site (62.196 °N, 174.674 °W) located ~37 km to the east of the 80 m echosounder mooring (Stabeno et al. 2012, Stabeno et al. 2023). In addition, PMEL deployed two ADCPs on the 100 and 120 m echosounder moorings. Current measurements (60 min by 4 m bins, see Stabeno et al. 2016 for methods) from the ADCPs (Teledyne RD Instruments, 300 kHz) during the period of the echosounder mooring deployments indicate that current speeds perpendicular to the maritime boundary did not exhibit the winter southeastward movement observed in the tracks (Fig. 8). This is consistent with long term observations and models of the current direction in this region showing year-round transport to the northwest along the depth contours of the shelf slope (Danielson et al. 2014, Stabeno et al. 2016). Pollock movement in winter cannot be explained by the prevailing currents (Fig. 8), and is thus attributed to active migration.

Further, if advection is the primary driver of movement, one would expect all sizes of fish to experience similar transport. We found that the direction of weaker scatterers (i.e. smaller fish) was consistent with those of stronger scatterers (Fig. S10). However, stronger scatterers tended to move faster (Figs S4, S5), consistent with onotogentic increases in swimming ability (Brodeur 1998, Hurst 2007). Thus, while their migration patterns are similar, swimming ability likely contributed to age-dependent differences in effective area occupied (Stevenson et al. 2022) and migration extent (Kotwicki et al. 2005). Together, the observations likely represent active migration between summer feeding and winter spawning distributions as exhibited by other gadid species (Rose et al. 1995, Ressler et al. 2007).

Acoustic estimates of pollock size

Although there was no biological sampling associated with the mooring deployments, inferences drawn from observed TSs correspond with pollock sizes reported from the summer fishery in both the US and Russian zones near the moorings. The pollock fishery on the Russian side of the border in summer 2019 and 2020 was concentrated between 100 and 200 m with catches primarily composed of adult pollock with a mean length of ~45 cm in both years (Gritsay and Stapenanko 2022). On the US portion of the shelf, fishery catches exhibited similar length distributions (Ianelli et al. 2022). The mooring observations of TS are consistent with reports from both management zones, in particular, the distributions of TSs observed in early summer 2020 which were dominated by scatterers whose TSs correspond to pollock ~40–50 cm in length

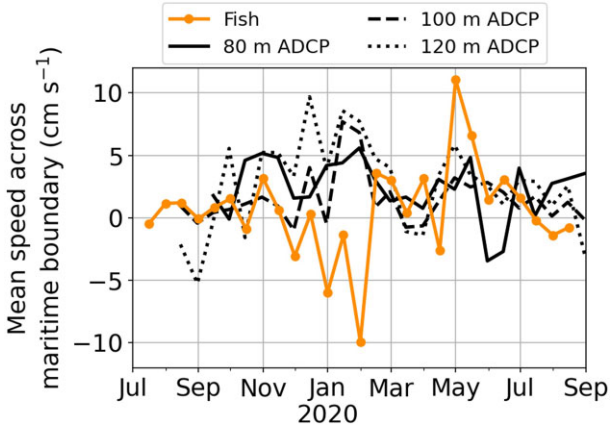

Figure 8. Comparison of mean fish speeds (orange line, mean V_R across all sizes and all sites, see methods) and current speeds (black lines) across the US–Russia maritime boundary during each semi-monthly period. Positive values indicate movement into Russia and those with negative values indicate movement into the US. Current speeds were calculated from hourly acoustic Doppler current profiler observations collected at M8 (~37 km east of 80 m mooring, here labeled as '80 m ADCP'), the 100 m, and 120 m mooring sites.

(Fig. 4). The moorings also observed TSs consistent with sizes expected from the 2018 cohort (−49 to −44 dB re 1 m^{-2} corresponding to 6–11 cm pollock) which were prevalent in the Bering Sea in 2019 (Ianelli et al. 2020). The steadily increasing TS between late fall and winter of this weaker mode of targets likely represents growth (Levine et al. 2021) of this age-1 cohort.

Long-term TS observations can be used to provide new insights into population dynamics such as the estimation of *in situ* growth rates (Levine et al. 2021) and identification of shifts in species and size composition (Sato et al. 2015, Kitamura et al. 2017, Levine et al. 2023). In contrast to mobile survey-based measurements, moorings allow for fish to be tracked over long periods as they move past the stationary platforms. The tracks analyzed in this study had a mean of 15 detections and a mean time in the acoustic beam of 11 s. Averaging many observations from a single fish greatly reduces the variance in the estimate of the TS (Ehrenberg and Torkelson 1996), providing greater confidence in our estimate of size than would be possible from a moving platform collecting relatively few observations from a single fish. While we use TS to identify relative changes in fish sizes over the course of the deployment, further validation is needed to verify that the length-class assignment of the GMM provides accurate inferences of length distributions from acoustic observations. Pollock TS is proportional to squared length (Lauffenburger et al. 2023), thus this method may be better suited for smaller fish where a given increase in length corresponds to larger changes in TS. If substantiated, analysis of TS distributions from tracked targets may allow for inference of size distribution in regions where the composition of scatterers is well classified and dominated by a single species with a well-constrained TS-length relationship (De Robertis et al. 2021, Levine et al. 2023).

Temperature effects on seasonal distribution

Our study supports the hypothesis that pollock movements are associated with the seasonal transitions in temperature. Seasonal spawning and feeding migrations have been inferred from synoptic acoustic- and bottom-trawl surveys (Stepananko 2001, Kotwicki et al. 2005, Kuznetsov et al. 2006), but the mechanism and timing of the migrations has remained poorly characterized. Our mooring observations provide direct evidence for a dominant northwest–southeast axis of migration largely along depth contours consistent with what has been inferred from seasonal changes in distribution (De Robertis and Cokelet 2012) and summer observations (Kotwicki et al. 2005, Stevenson et al. 2022). The observations indicate that the southeast and northwest migrations are largely restricted to the winter and late spring, respectively. In the Bering Sea, pollock primarily spawn from February to May (Hinckley 1987, Bacheler et al. 2010). Thus, the fish moving into the US zone in the winter are likely spawning in US waters.

Our moorings were deployed at the end of an extreme warming period across the Bering Sea shelf (Stabeno and Bell 2019, Eisner et al. 2020), during which pollock abundance was high in the western Bering Sea (Gritsay and Stepanenko 2022, O'Leary et al. 2022). As proposed by Eisner et al. (2020), a multiyear warming trend and low sea ice in 2019 may have led to the development of a "thermal corridor" for the large-scale migration. We hypothesize that warming may have led to increased northwest migration of pollock into Russian waters (Fig. 9, red region). As the shelf cooled from the north in winter, pollock then retreated southeast into the warmer water present over southern portions of the US shelf (purple region, Fig. 9) and possibly the deeper areas of the shelf slope. During the subsequent summer of 2020, water temperatures in the region of the moorings were moderate compared to previous years (Fig. S11). Pollock encountered cooler waters and therefore did not migrate as extensively into Russian waters due to a reduced thermal corridor (blue region, Fig. 9).

This pattern of temperature-mediated migration is consistent with previous analyses of the relationship between pollock and temperature in the eastern Bering Sea. The area occupied by pollock on the eastern Bering Sea shelf has a negative relationship with the extent of the cold pool (Stevenson et al. 2022), and adult pollock are known to avoid cold temperatures (Wyllie-Echerverria and Wooster 1998, Kotwicki et al. 2005, Kotwicki and Lauth 2013). During the recent period of extreme warming, pollock migrated more extensively into Russia and the northern Bering Sea compared to previous years (Stevenson and Lauth 2019, Eisner et al. 2020, O'Leary et al. 2022). Pollock catches in the western Bering Sea increased in 2019, which has been attributed to increased migration from the eastern Bering Sea due to warming of the shelf (Basyuk and Zuenko 2020, Gritsay and Stepananeko 2022). The US fishery also reported increased effort in the northwestern region of the eastern shelf (Ianelli et al. 2020). When temperatures cooled in 2020, pollock abundance was reduced in the northwestern portion of the Bering Sea (Polyanichko and Kuznetzov 2022), consistent with the mooring observations of net movement into the US during the deployment period.

Pollock distribution under continued warming

Globally, continued ocean warming is anticipated to further disrupt transboundary fisheries, creating mismatches between species distributions and the allocation and management of

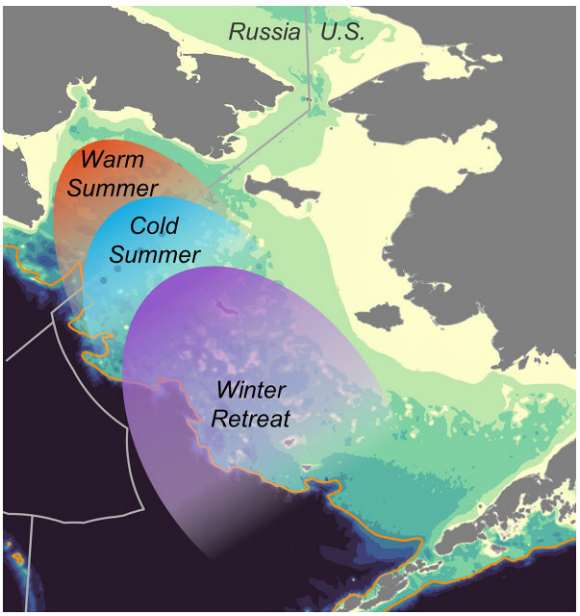

Figure 9. Diagram of the hypothesized shift in the northwest leading edge of the pollock population crossing the US–Russia maritime boundary due to interannual temperature variability. In warm years (i.e. 2019, red region), more of the pollock population migrates well into the Russian portion of the Bering Sea shelf. In winter (purple region), the population retreats to warmer waters along the shelf slope and the southeastern Bering Sea. In cooler years (i.e. 2020, blue region), the summer transboundary migration is reduced and fewer pollock enter Russian waters. The 200 m contour is indicated by the orange line.

the species across borders (Pinsky et al. 2018, Maureaud et al. 2021, Palacios-Abrantes et al. 2022). The Bering Sea is undergoing rapid warming and is predicted to warm by as much as 2.5°C–5.0°C by 2100 (Hermann et al. 2019). Thus, we anticipate that exchange of pollock across US and Russian national boundaries will continue to increase over future decades. As warming continues, the timing and magnitude of pollock transboundary migration is likely to change as pollock begin their spring migration earlier or continue to shift their distribution northward. Such a shift is already occurring as evidenced by the increasing catches in the northwest portion of the US management region (Ianelli et al. 2020) and large numbers of pollock present in the northern Bering Sea in summer (Eisner et al. 2020). In addition to changing the transboundary allocation of the stock, this will also lead to further misalignment between the area occupied and the coverage of surveys designed to cover historic distribution patterns (Levine and De Robertis 2019, O'Leary et al. 2020).

The population movements described here may provide evidence of how changes in temperature on the Being Sea shelf may directly impact fisheries assessments. In 2018, during the peak the recent warm period (2017–2019), pollock backscatter observed during the biennial eastern Bering Sea acoustic-trawl survey decreased by ~50% from the previous two surveys, with substantial biomass observed at the northwest survey boundaries (McCarthy et al. 2020, De Robertis et al. 2021). This may have been partially due to reduced availability of pollock in the survey area as the population moved into the western and northern Bering Sea (Eisner et al. 2020, O'Leary et al. 2020). A temperature-driven shift has been identified in pollock based on summer bottom-trawl surveys where pollock availability to the survey and the fishery in the eastern Bering Sea has been reduced during recent warm years (Ianelli et al. 2019, O'Leary et al. 2022). Additionally, there is evidence that pollock have recently moved beyond the Bering Strait into Arctic waters (Maznikova et al. 2023), further complicating management of the species.

Conclusions

Direct observation of walleye pollock movement indicates that there is substantial seasonal movement of the population across the US–Russia maritime boundary. A portion of the pollock stock appears to migrate from the eastern Bering Sea into Russian waters in late spring and return to the eastern Bering Sea in winter. The extent of pollock movement between zones appears to be at least partially driven by temperature. This suggests that years where the northern Bering Sea shelf is warmer will result in a greater portion of the stock entering Russian waters.

From a management perspective, mooring observations may further inform hypotheses for future pollock spatial and temporal distributions so that robust monitoring and catch control rules can be developed and tested in response to known spatiotemporal stock trends and the environmental drivers of those trends. A mechanistic understanding of pollock movement can be incorporated into climate-enhanced assessment models, or provide further insight into fine-scale vertical distribution (Monnahan et al. 2021) and horizontal movements to further improve the assessment used in management advice (Ianelli et al. 2022). For example, a key question is how much of the stock is available to the summer acoustic- and bottom-trawl surveys of the US portion of the eastern Bering Sea, and this could be addressed with further years of mooring observations. Additional years of observation as well as expanded spatial coverage such as the placement of additional moorings further north into the northern Bering Sea or deeper along the shelf slope would also help identify future shifts in pollock movement that impact summer distributions. Mooring-based observations of transboundary migration can be assimilated with other data, such as additional *in situ* measurements of environmental parameters and predictions from climate and circulation models, to better inform models of fish population movement across larger spatial and temporal scales (Thorson et al. 2021). While there are limitations to spatially explicit assessment models, the direct inclusion of movement and the mechanisms that drive changes in pollock distribution can help to more accurately predict changes in biomass on a regional basis (Hulson et al. 2013). Given that the eastern Bering Sea is predicted to continue warming (Hermann et al. 2019), we anticipate that the degree to which pollock migrate across the maritime boundary into Russia will increase. Thus, understanding the mechanisms driving pollock migrations will become increasingly important for management of this important transboundary stock.

Acknowledgements

The mooring deployments would not have been possible without the captains, crews, and science parties of the bottom-trawl survey on the FV *Alaska Knight*. Sarah Donohoe, Catherine Berchok, and the crew of the NOAA ship *Oscar Dyson* recovered the moorings at the height of the

COVID-19 pandemic under exceedingly difficult conditions. We thank Chris Wilson for encouragement and Phyllis Stabeno and Shaun Bell for providing the processed CTD data. We thank Sam Urmy, Nathan Lauffenburger, Cecilia O'Leary, and Sandra Parker-Stetter who provided comments on the early drafts of this work. Any use of trade, firm, or product names is for descriptive purposes only and does not imply endorsement by the US Government. Findings of this paper do not necessarily represent the views of the National Oceanic and Atmospheric Administration.

Author contributions

A.D.R. conceived of the project. A.D.R., J.N.I. and C.B. managed the funding acquisition and project administration. A.D.R. and M.L. conducted the retrospective analysis to identify mooring locations and the fieldwork. R.M.L., AD.R., and C.B. contributed to the methodology and R.M.L. led the data analysis. R.M.L. led the writing of the manuscript and all authors contributed to review and editing.

Supplementary material

Supplementary data is available at *ICES Journal of Marine Science* online.

Conflict of interest: The authors declare that they have no conflict of interest.

Funding

This work was funded by the Alaska Fisheries Science Center's Regional Work Plan.

Data availability

All echosounder data, including calibration information, are available via the Water Column Sonar Data archive at the NOAA National Centers for Environmental Information at the following DOIs: https://doi.org/10.25921/qc84-dy18, https://doi.org/10.25921/7g5g-gb35, https://doi.org/10.25921/vvka-tf34, https://doi.org/10.25921/crvy-s144.

References

Bacheler NM, Ciannelli L, Bailey KM *et al.* Spatial and temporal patterns of walleye pollock (*Theragra chalcogramma*) spawning in the eastern Bering Sea inferred from egg and larval distributions. *Fish Oceanogr 2010*;**19**:107–20. https://doi.org/10.1111/j.1365-2419.2009.00531.x

Bailey KM, Quinn TJ, Bentzen P *et al.* Population structure and dynamics of walleye pollock, *Theragra chalcogramma*. *Adv Mar Biol 1999*;**37**:179–255. https://doi.org/10.1016/S0065-2881(08)60429-0

Basyuk E, Zuenko Y. Extreme oceanographic conditions in the northwestern Bering Sea in 2017–2018. *Deep Sea Res Part II 2020*;**181–2**:104909.

Blackman SS. *Multiple-target Tracking with Radar Applications*. Dedham, MA: Artech House, Inc., 1986, 463.

Brodeur RD. Prey selection by age-0 walleye pollock, *Theragra chalcogramma*, in nearshore waters of the Gulf of Alaska. *Environ Biol Fishes 1998*;**51**:175–86. https://doi.org/10.1023/A:1007455619363

Christiansen S, Langangen Ø, Titelman J *et al.* Three-dimensional swimming behavior and activity of a mesopelagic fish. *Limnol Oceanogr 2022*;**67**:2677–90. https://doi.org/10.1002/lno.12230

Clement Kinney J, Maslowski W, Osinski R *et al.* On the variability of the Bering Sea Cold Pool and implications for the biophysical environment. *PLoS One 2022*;**17**:e0266180. https://doi.org/10.1371/journal.pone.0266180

Currie JC, Thorson JT, Sink KJ *et al.* A novel approach to assess distribution trends from fisheries survey data. *Fish Res 2019*;**214**:98–109. https://doi.org/10.1016/j.fishres.2019.02.004

Danielson SL, Weingartner TJ, Hedstrom KS *et al.* Coupled wind-forced controls of the Bering–Chukchi shelf circulation and the Bering Strait throughflow: ekman transport, continental shelf waves, and variations of the Pacific–Arctic sea surface height gradient. *Prog Oceanogr 2014*;**125**:40–61. https://doi.org/10.1016/j.pocean.2014.04.006

Demer DA, Berger L, Bernasconi M *et al.* Calibration of acoustic instruments. *ICES Coop Res Rep 2015*;**326**:133.

De Robertis A, Cokelet ED. Distribution of fish and macrozooplankton in ice-covered and open-water areas of the eastern Bering Sea. *Deep Sea Res Part II 2012*;**65–70**:217–29. https://doi.org/10.1016/j.dsr2.2012.02.005

De Robertis A, Levine M, Lauffenburger N *et al.* Uncrewed surface vehicle (USV) survey of walleye pollock, *Gadus chalcogrammus*, in response to the cancellation of ship-based surveys. *ICES J Mar Sci 2021*;**78**:2797–808. https://doi.org/10.1093/icesjms/fsab155

De Robertis A, Levine R, Wilson CD. Can a bottom-moored echo sounder array provide a survey-comparable index of abundance? *Can J Fish Aquat Sci 2018*;**75**:629–40. https://doi.org/10.1139/cjfas-2017-0013

Ehrenberg JE, Torkelson TC. Application of dual-beam and split-beam target tracking in fisheries acoustics. *ICES J Mar Sci 1996*;**53**:329–34. https://doi.org/10.1006/jmsc.1996.0044

Eisner LB, Zuenko YI, Basyuk EO *et al.* Environmental impacts on walleye pollock (*Gadus chalcogrammus*) distribution across the Bering Sea shelf. *Deep Sea Res Part II 2020*;**181–182**:104881. https://doi.org/10.1016/j.dsr2.2020.104881

FAO. FAO Yearbook. Fishery and aquaculture statistics 2019. Rome: FAO, 2021.

Fetterer F, Stewart JS, Meier WN. *MASAM2: Daily 4 Km Arctic Sea Ice Concentration, Version 2*. Boulder, CO: NSIDC: National Snow and Ice Data Center, 2023.

Gritsay EV, Stepanenko MA. Oceanographic conditions and analysis of walleye pollock *theragra chalcogramma* fishery in the Navarin area in 2017–2021. *Izv TINRO 2022*;**202**:535–55. https://doi.org/10.26428/1606-9919-2022-202-535-555

Hermann AJ, Gibson GA, Cheng W *et al.* Projected biophysical conditions of the Bering Sea to 2100 under multiple emission scenarios. *ICES J Mar Sci 2019*;**76**:1280–304. https://doi.org/10.1093/icesjms/fsz111

Hinckley S. The reproductive biology of walleye pollock, *theragra chalcogramma*, in the Bering Sea, with reference to spawning stock structure. *Fish Bull 1987*;**85**:481–98

Honkalehto T, Ressler PH, Towler RH *et al.* Using acoustic data from fishing vessels to estimate walleye pollock (*Theragra chalcogramma*) abundance in the eastern Bering Sea. *Can J Fish Aquat Sci 2011*;**68**:1231–42. https://doi.org/10.1139/f2011-050

Hulson PF, Quinn TJ, Hanselman DH *et al.* Spatial modeling of Bering Sea walleye pollock with integrated age-structured assessment models in a changing environment. *Can J Fish Aquat Sci 2013*;**70**:1402–16. https://doi.org/10.1139/cjfas-2013-0020

Hurst TP. Thermal effects on behavior of juvenile walleye pollock (*Theragra chalcogramma*): implications for energetics and food web models. *Can J Fish Aquat Sci 2007*;**64**:449–57. https://doi.org/10.1139/f07-025

Ianelli J, Fissel B, Holsman K *et al.* Assessment of the walleye pollock stock in the Eastern Bering Sea. *North Pacific Stock Assessment and Fishery Evaluation Report*. 2019, 169. Available at https://www.fisheries.noaa.gov/resource/data/2019-assessment-walleye-pollock-stock-eastern-bering-sea (30 July 2023, date last accessed).

Ianelli J, Fissel B, Holsman K *et al.* Assessment of the walleye pollock stock in the Eastern Bering Sea. *North Pacific Stock*

Assessment and Fishery Evaluation Report. 2020, 173. Available at https://www.fisheries.noaa.gov/resource/data/2020-assessment-walleye-pollock-stock-eastern-bering-sea (30 July 2023, date last accessed).

Ianelli J, Stienessen S, Honkalehto T *et al.* Assessment of the walleye pollock stock in the Eastern Bering Sea. *North Pacific Stock Assessment and Fishery Evaluation Report*. 2022, 160. Available at https://www.fisheries.noaa.gov/resource/data/2022-assessment-walleye-pollock-stock-eastern-bering-sea (30 July 2023, date last accessed).

Kaartvedt S, Røstad A, Klevjer TA *et al.* Use of bottom-mounted echo sounders in exploring behavior of mesopelagic fishes. *Mar Ecol Prog Ser 2009*;**395**:109–118. https://doi.org/10.3354/meps08174

Kitamura M, Amakasu K, Kikuchi T *et al.* Seasonal dynamics of zooplankton in the southern Chukchi Sea revealed from acoustic backscattering strength. *Cont Shelf Res 2017*;**133**:47–58. https://doi.org/10.1016/j.csr.2016.12.009

Kotwicki S, Buckley TW, Honkalehto T *et al.* Variation in the distribution of walleye pollock (*Theragra chalcogramma*) with temperature and implications for seasonal migration. *Fish Bull 2005*;**103**:574–87.

Kotwicki S, De Robertis A, von Szalay P *et al.* The effect of light intensity on the availability of walleye pollock (Theragra chalcogramma) to bottom trawl and acoustic surveys. *Can J Fish Aquat Sci 2009*;**66**:983–94. https://doi.org/10.1139/F09-055

Kotwicki S, Lauth RR. Detecting temporal trends and environmentally-driven changes in the spatial distribution of bottom fishes and crabs on the eastern Bering Sea shelf. *Deep Sea Res Part II 2013*;**94**:231–43. https://doi.org/10.1016/j.dsr2.2013.03.017

Kuznetsov MY, Efimkin AJ, Basyuk E. Distribution and habitat conditions of walleye pollock in the Navarin–Anadyr region of Bering Sea in summer–autumn, 2002–2003. *Izv TINRO 2006*;**144**:247–64.

Lauffenburger N, De Robertis A, Williams K *et al.* Mining previous acoustic surveys to improve walleye pollock (*Gadus chalcogrammus*) target strength estimates. *ICES J Mar Sci 2023*;**80**:1683–96. https://doi.org/10.1093/icesjms/fsad094

Levine M, De Robertis A. Don't work too hard: subsampling leads to efficient analysis of large acoustic datasets. *Fish Res 2019*;**219**:105323. https://doi.org/10.1016/j.fishres.2019.105323

Levine RM, De Robertis A, Grünbaum D *et al.* Autonomous vehicle surveys indicate that flow reversals retain juvenile fishes in a highly advective high-latitude ecosystem. *Limnol Oceanogr 2021*;**66**:1139–54. https://doi.org/10.1002/lno.11671

Levine RM, De Robertis A, Grünbaum D *et al.* Transport-driven seasonal abundance of pelagic fishes in the Chukchi Sea observed with seafloor-mounted echosounders. *ICES J Mar Sci 2023*;**80**:987–1001. https://doi.org/10.1093/icesjms/fsad024

Liu OR, Molina R. The persistent transboundary problem in marine natural resource management. *Front Mar Sci 2021*;**8**:656023. https://doi.org/10.3389/fmars.2021.656023

Maathuis MAM, Couperus B, van der Molen J *et al.* Resolving the variability in habitat use by juvenile small pelagic fish in a major tidal system by continuous echosounder measurements. *Mar Ecol Prog Ser 2023*;**SPFav4**. https://doi.org/10.3354/meps14368

Maeda T. Life cycle and behavior of adult pollock (*Theragra chalcogramma* (Pallas)) in waters adjacent to Funka Bay, Hokkaido Island. *Int North Pac Fish Comm Bull 1986*;**45**:39–65.

Maureaud AA, Frelat R, Pecuchet L *et al.* Are we ready to track climate-driven shifts in marine species across international boundaries?—A global survey of scientific bottom trawl data. *Glob Change Biol 2021*;**27**:220–36. https://doi.org/10.1111/gcb.15404

Maznikova OA, Emelin PO, Sheibak AY *et al.* Can an invader support commercial fishing? A case study of walleye pollock *gadus chalcogrammus* in the western Chukchi Sea. *Deep Sea Res Part II 2023*;**207**:105222. https://doi.org/10.1016/j.dsr2.2022.105222

McCarthy A, Honkalehto T, Lauffenburger N *et al.* Results of the acoustic-trawl survey of walleye pollock (*Gadus chalcogrammus*) on the U.S. Bering Sea Shelf in June-August 2018 (DY1807). 2020, 83, AFSC Processed Report, 2020-07, Alaska Fish. Sci. Cent., NOAA, Natl. Mar. Fish. Serv., 7600 Sand Point Way NE, Seattle WA 98115.

McLachlan G, Peel D. *Finite Mixture Models*. Brisbaine: John Wiley & Sons, Inc., 2000, 419.

Melbourne-Thomas J, Audzijonyte A, Brasier MJ *et al.* Poleward bound: adapting to climate-driven species redistribution. *Rev Fish Biol Fish 2022*;**32**:231–51. https://doi.org/10.1007/s11160-021-09641-3

Meltzer E. Global overview of straddling and highly migratory fish stocks—the nonsustainable nature of High Seas fisheries. *Ocean Dev Int Law 1994*;**25**:255–344. https://doi.org/10.1080/00908329409546036

Miller KA, Munro GR. Climate and Cooperation: a new perspective on the management of shared fish stocks. *Mar Res Econ 2004*;**19**:367–93. https://doi.org/10.1086/mre.19.3.42629440

Monnahan CC, Thorson JT, Kotwicki S *et al.* Incorporating vertical distribution in index standardization accounts for spatiotemporal availability to acoustic and bottom trawl gear for semi-pelagic species. *ICES J Mar Sci 2021*;**78**:1826–39. https://doi.org/10.1093/icesjms/fsab085

O'Leary CA, DeFilippo LB, Thorson JT *et al.* Understanding transboundary stocks' availability by combining multiple fisheries-independent surveys and oceanographic conditions in spatiotemporal models. *ICES J Mar Sci 2022*;**79**:1063–74. https://doi.org/10.1093/icesjms/fsac046

O'Leary CA, Thorson JT, Ianelli JN *et al.* Adapting to climate-driven distribution shifts using model-based indices and age composition from multiple surveys in the walleye pollock (*Gadus chalcogrammus*) stock assessment. *Fish Oceanogr 2020*;**29**:541–57. https://doi.org/10.1111/fog.12494

Ona E, Mitson RB. Acoustic sampling and signal processing near the seabed: the deadzone revisited. *ICES J Mar Sci 1996*;**53**:677–90. https://doi.org/10.1006/jmsc.1996.0087

Palacios-Abrantes J, Frolicher TL, Reygondeau G *et al.* Timing and magnitude of climate-driven range shifts in transboundary fish stocks challenge their management. *Glob Change Biol 2022*;**28**:2312–26. https://doi.org/10.1111/gcb.16058

Parker-Stetter SL, Horne JK, Urmy SS *et al.* Vertical distribution of age-0 walleye pollock during late summer: environment or ontogeny? *Mar Coast Fish 2015*;**7**:349–69. https://doi.org/10.1080/19425120.2015.1057307

Pinsky ML, Reygondeau G, Caddell R *et al.* Preparing ocean governance for species on the move. *Science 2018*;**360**:1189–91. https://doi.org/10.1126/science.aat2360

Pinsky ML, Worm B, Fogarty MJ *et al.* Marine taxa track local climate velocities. *Science 2013*;**341**:1239–42. https://doi.org/10.1126/science.1239352

Polyanichko VI, Kuznetsov MY. Distribution and abundance of walleye pollock *theragra chalcogramma* in the northwestern Bering Sea in the summer-fall period of 2020 and their interannual variability. *Izv TINRO 2022*;**202**:793–809. https://doi.org/10.26428/1606-9919-2022-202-793-809

Radchenko VI, Sobolevskiy YI. Seasonal spatial distribution dynamics of walleye pollock in the Bering Sea. *J Ichthyol 1993*;**33**:63–76.

Ressler PH, Holmes JA, Fleischer GW *et al.* Pacific hake, *Merluccius productus*, autecology: a timely review. *Mar Fish Rev 2007*;**69**:1–24.

Rose GA, deYoung B, Colbourne EB. Cod (*Gadus morhua* L.) migration speeds and transport relative to currents on the north-east Newfoundland Shelf. *ICES J Mar Sci 1995*;**52**:903–13. https://doi.org/10.1006/jmsc.1995.0087

Sato M, Horne JK, Parker-Stetter SL *et al.* Acoustic classification of coexisting taxa in a coastal ecosystem. *Fish Res 2015*;**172**:130–36. https://doi.org/10.1016/j.fishres.2015.06.019

Shaw CT, Bi H, Feinberg LR *et al.* Cohort analysis of *Euphausia pacifica* from the Northeast Pacific population using a gaussian mixture model. *Prog Oceanogr 2021*;**191**:102495. https://doi.org/10.1016/j.pocean.2020.102495

Shchepetkin AF, McWilliams JC. The regional oceanic modeling system (ROMS): a split-explicit, free-surface, topography-following-coordinate oceanic model. *Ocean Modell 2005*;**9**:347–404. https://doi.org/10.1016/j.ocemod.2004.08.002

Stabeno P, Bell S, Berchok C *et al*. Long-term biophysical observations and climate impacts in US arctic marine ecosystems. *Oceanography 2023*;**36**:78–85

Stabeno PJ, Bell SW. Extreme Conditions in the Bering Sea (2017–2018): record-breaking low sea-ice extent. *Geophys Res Lett 2019*;**46**:8952–59. https://doi.org/10.1029/2019GL083816

Stabeno PJ, Danielson SL, Kachel DG *et al*. Currents and transport on the Eastern Bering Sea shelf: an integration of over 20 years of data. *Deep Sea Res Part II 2016*;**134**:13–29. https://doi.org/10.1016/j.dsr2.2016.05.010

Stabeno PJ, Farley EV, Kachel NB *et al*. A comparison of the physics of the northern and southern shelves of the eastern Bering Sea and some implications for the ecosystem. *Deep Sea Res Part II 2012*;**65–70**:14–30. https://doi.org/10.1016/j.dsr2.2012.02.019

Stepanenko MA. Relationship between age and spatial distribution of walleye pollock *theragra chalcogramma* in the eastern and northwestern Bering Sea. *Izv TINRO 2001*;**128**:125–35.

Stevenson DE, Kotwicki S, Thorson JT *et al*. The influence of age and cohort on the distribution of walleye pollock (*Gadus chalcogrammus*) in the eastern Bering Sea. *Can J Fish Aquat Sci 2022*;**79**:1934–49. https://doi.org/10.1139/cjfas-2021-0300

Stevenson DE, Lauth RR. Bottom trawl surveys in the northern Bering Sea indicate recent shifts in the distribution of marine species. *Polar Biol 2019*;**42**:407–21. https://doi.org/10.1007/s00300-018-2431-1

Thorson JT, Barbeaux SJ, Goethel DR *et al*. Estimating fine-scale movement rates and habitat preferences using multiple data sources. *Fish Fish 2021*;**22**:1359–76. https://doi.org/10.1111/faf.12592

Traynor JJ. Target-strength measurements of walleye pollock (*Theragra chalcogramma*) and Pacific whiting (*Merluccius productus*). *ICES J Mar Sci 1996*;**53**:253–58. https://doi.org/10.1006/jmsc.1996.0031

Trevorrow MV. The use of moored inverted echo sounders for monitoring meso-zooplankton and fish near the ocean surface. *Can J Fish Aquat Sci 2005*;**62**:1004–18. https://doi.org/10.1139/f05-013

Urmy SS, Horne JK, Barbee DH. Measuring the vertical distributional variability of pelagic fauna in Monterey Bay. *ICES J Mar Sci 2012*;**69**:184–96. https://doi.org/10.1093/icesjms/fsr205

Woillez M, Poulard JC, Rivoirard J *et al*. Indices for capturing spatial patterns and their evolution in time, with application to European hake (*Merluccius merluccius*) in the Bay of Biscay. *ICES J Mar Sci 2007*;**64**:537–550. https://doi.org/10.1093/icesjms/fsm025

Wyllie-Echeverria T, Wooster WS. Year to-year variations in Bering Sea ice cover and some consequences for fish distributions. *Fish Oceanogr 1998*;**7**:159–70. https://doi.org/10.1046/j.1365-2419.1998.00058.x

Handling Editor: Richard O'Driscoll